Plasmon mediated cathodic photocurrent generation in sol-gel synthesized doped $SrTiO_3$ nanofilms

Ramu Pasupathi Sugavaneshwar, Kai Chen, Gandham Lakshminarayana, Satoshi Ishii, Thang Duy Dao, Naoto Umezawa, and Tadaaki Nagao

Citation: APL Materials **3**, 116103 (2015); doi: 10.1063/1.4935305
View online: https://doi.org/10.1063/1.4935305
View Table of Contents: http://aip.scitation.org/toc/apm/3/11
Published by the American Institute of Physics

Plasmon mediated cathodic photocurrent generation in sol-gel synthesized doped $SrTiO_3$ nanofilms

Ramu Pasupathi Sugavaneshwar,[1,2,a] Kai Chen,[1,2]
Gandham Lakshminarayana,[1,2] Satoshi Ishii,[1,2] Thang Duy Dao,[1,2]
Naoto Umezawa,[2,3] and Tadaaki Nagao[1,2,a]
[1]*International Center for Materials Nanoarchitectonics (MANA), National Institute for Materials Science (NIMS), 1-1 Namiki, Tsukuba, Ibaraki 305-0044, Japan*
[2]*CREST, Japan Science and Technology Agency, 4-1-8 Honcho, Kawaguchi, Saitama 332-0012, Japan*
[3]*Catalytic Materials Group, Environmental Remediation Materials Unit, National Institute for Materials Science (NIMS), 1-1 Namiki, Tsukuba, Ibaraki 305-0044, Japan*

(Received 15 May 2015; accepted 21 October 2015; published online 5 November 2015)

Thin films of $SrTiO_3$ (STO) and Rh-doped $SrTiO_3$ (Rh-STO) were synthesized by sol-gel method and loaded with Ag nanoparticles. Pristine STO films exhibited anodic photocurrent while Rh-STO exhibited cathodic photocurrent. An enhancement in the overall cathodic photocurrent is observed with Ag nanoparticle loading and an additional enhancement in the visible light range is seen from the incident photon-to-current efficiency spectrum due to synergetic effect of Rh doping and Ag loading in STO. [http://dx.doi.org/10.1063/1.4935305]

Photoelectrochemical (PEC) reaction pioneered by Fujishima and Honda has widely emerged as a potential approach to convert solar energy into chemical energy.[1] Traditionally, various oxide materials, such as TiO_2,[2] ZnO,[3] and Fe_2O_3,[4] have been investigated as candidates for solar energy conversion materials but their ability is limited by the positions of band edges with respect to the redox potentials, weak optical absorption in the visible light range, or short lifetimes of photo-excited carriers.[5–7] Recently, $SrTiO_3$ (STO) has been widely investigated for photocatalytic water splitting since both hydrogen and oxygen evolution reactions are possible without applying an external bias potential. However, its ability to harness visible light is impeded since its band gap lies in the UV region.[8–10] Various efforts have been taken to improve the visible light harnessing ability of the STO by doping with transition elements such as Cr^{3+}, La^{3+}, and Rh^{4+}.[10–14] Particularly, Rh doping has generated interest not only for improving the visible light harnessing ability, but also inducing p-type nature in the electrochemical reaction producing cathodic photocurrent.[14–17]

In addition, visible light harvesting ability of the oxides semiconductors can be enhanced with the incorporation of metal nanoparticles (NPs).[18–20] It has been shown that the localized surface plasmon resonances (LSPRs) exhibited by the metal nanoparticles create strong local electric field at the metal/oxide interfaces, which promotes the concentration of photon energy at the interfaces and provides sufficient energy to inject electrons from metal nanoparticles into semiconductors. This mechanism enables light absorption in the visible light range and is termed as *hot electron injection* that has been successfully applied to Au/TiO_2, $Au/SrTiO_3$, etc., in enhancing the anodic photocurrent in oxide semiconductors.[18–24]

However, the role of metal nanoparticles in visible light harvesting ability and cathode photocurrent enhancement has not been fully explored yet. Here, we investigate the effects of Rh doping on the structural as well as optical properties of STO thin films and plasmon-enhanced photocurrent

[a]Authors to whom correspondence should be addressed. Electronic addresses: r.p.sugavaneshwar@nims.go.jp and NAGAO.Tadaaki@nims.go.jp. Telephone: +81-29-860-4746. Fax: +81-29-860-4793.

with Ag nanoparticle loading. We conclude that Rh doping and coupling with Ag nanoparticles can effectively enhance the cathodic photocurrent in the visible region.

Rh doped STO nanofilm (Rh-STO) is prepared as follows. STO precursor solutions were prepared using strontium acetate hemihydrate and titanium tetra-*n*-butoxide as starting materials, and acetic acid, 2-methoxyethanol, and acetylacetone as solvents. Strontium acetate was initially dissolved in glacial acetic acid denoted as solution A and was stirred for 1 h at 60 °C. Titanium tetra-*n*-butoxide mixed with 2-methoxyethanol and acetylacetone denoted as solution B was stirred separately at 25 °C for 1 h. Solution B was then added to solution A dropwise under constant stirring and the mixture was then stirred at 60 °C for 1 h. For rhodium doping, stoichiometric amount of rhodium oxide is added to the solution to obtain the ratio ($Sr_{0.95}$, $Rh_{0.05}$) TiO_3. Here, we attempted Sr site substitution for Rh doping which has not been investigated very much compare to Ti site. The obtained solution was spin-coated on Si substrate; ITO glass and wet films were left to dry at 60 °C for 12 h. In order to crystallize, the films were annealed at 600 °C for 1 h. It is noted that the current fabrication method yields highly two-dimensional film morphology as well as very smooth surfaces (roughness in r.m.s. 0.7 nm). Ag or Au plasmonic nanoparticles were fabricated on top of Rh-STO films by depositing Ag/Au film of 3 nm in thickness on Rh-STO films (Ag/Rh-STO and Au/Rh-STO) by thermal evaporation (in base pressure below 10^{-4} Torr) and then annealing the films at 300 °C in air and in N_2 for Au and Ag, respectively.

The morphology of the nanocomposites was characterized using a field emission scanning electron microscope (FE-SEM, Hitachi, 5 kV operating voltage). The crystal structures of the STO films were characterized by an X-ray diffractometer (XRD, smartlab, Cu Ka) with films coated on Si substrate. Optical transmittance of each sample was examined using a UV-VIS spectrometer (JASCO V-570) at room temperature. For the photocurrent measurements, a simple PEC cell was used, with photoelectrodes made from STO, Rh-STO, Ag/Rh-STO, and Au/Rh-STO. These STO and Rh-STO were spin coated on ITO substrates and annealed further after the deposition of Au or Ag to form NPs as described earlier. The annealed films were connected to a high-purity copper wire using silver paste, and an insulating epoxy layer was then used to cover all excess ITO surfaces on the edge of the ITO glass to prevent short-circuit currents. The PEC cell measurements were carried out with the catalyst photoelectrodes, a Pt zigzag wire acting as the counter electrode, and Na_2SO_4 solutions (0.5M) acting as the electrolyte. A standard AM 1.5 G solar simulator (JASCO Otentosun) with a power density of 100 mW/cm^2 was used as the light source for the PEC cell. For the wavelength dependent photocurrent measurements, a wavelength tunable light source (Bunkyukeoki, Niji2) was used.

XRD patterns of the STO and the Rh-STO films are shown in Figure S1(a) in the supplementary material.[32] The doped films have nearly the identical crystal structure as the pure STO film, indicating that doping Rh cations does not result in the formation of segregated Rh phase and the film is a single phase. A closer examination of the 110 peak of pure and Rh-STO films (Figure S1(b)[32]) reveals a noticeable peak shift towards the lower theta angle, which suggests a moderate lattice expansion caused by the doping. In our experiment, we intended to substitute Sr^{2+} (ionic radius 0.118 nm) with Rh^{3+} (ionic radius 0.080) in the STO lattice, but the observed XRD pattern shows lattice expansion contrary to our expectation. This fact strongly suggests that Rh^{3+} occupies Ti^{4+} (0.064 nm) sites, leaving Sr^{2+} vacancies.[9] Our preliminary calculation regarding the cohesive energy of the Rh-STO also supports this model. Also the excess Ti (smallest ion in the system) may have occupied interstitial sites which are supported by lattice expansion shown in the XRD. Figures 1(a)-1(d) show the SEM image of Rh-STO and STO with Au and Ag nanoparticle on it. Ag and Au NPs were uniformly dispersed and the probability for agglomeration or aggregation of the particles on the STO surface is not very high.

From UV-vis transmission spectra in Figure 1(e), strong absorption (transmission drop) was observed for all the samples in the UV region due to band to band transition for STO. The transmission spectrum for Rh-STO shows moderate increase in the absorption compared to STO in the near visible region indicating the formation of impurity levels in the band gap and the optical excitations involving these levels. Coupling with Ag NPs increases the visible light absorption of Ag/Rh-STO due to LSPR of Ag NPs while coupling with Au NPs and STO shows a separate absorption peak around 600 nm.

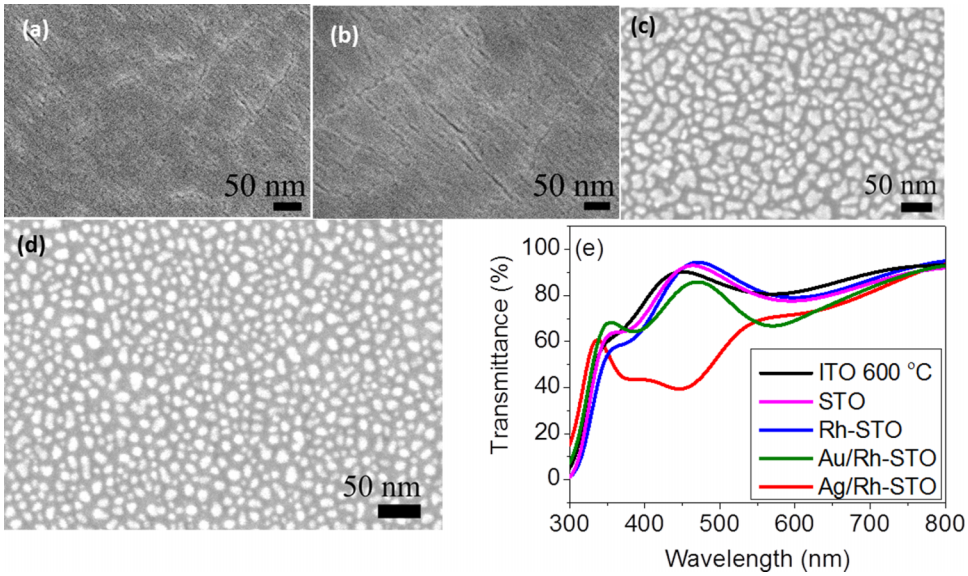

FIG. 1. SEM images of (a) STO, (b) Rh-STO, (c) Au/Rh-STO films, (d) Ag/Rh-STO, and (e) UV-vis transmission spectra of the various STO films. All the transmittance data were normalized to the transmittance of the unheated ITO glass.

The PEC measurement is presented in Figure 2. For all the photoelectrodes, the rise and fall of the photocurrent correspond to the switching of the illumination. This pattern of photocurrent was highly reproducible for more than ten cycles. The short-circuit photocurrent density of the STO photoelectrode is 0.12 μA/cm^2, and the photocurrent densities of Rh-STO, Ag/Rh-STO, and Au/Rh-STO photoelectrodes are 0.25, 0.6, and 0.19 μA/cm^2, respectively. Here, it should be noted that STO produces anodic photocurrent, while doping with Rh produces cathodic photocurrent. Furthermore, coupling with Ag NPs enhances the cathodic photocurrent by a factor of 2, while no significant enhancement in cathodic photocurrent is observed with Au NPs loading.

It is known that the photocurrent density can be affected by several factors. We carried out X-ray photoelectron spectroscopy (XPS) measurements to examine the valence states of Rh in Rh-doped STO nanofilms. The high-resolution Rh 3d spectrum shown in Figure 3(a) reveals that the doublet peaks at 313.1 and 308.1 eV, which are assigned to Rh^{3+} states.[17] Moreover, when we compare the Ti and Sr peaks in pristine STO to those in Rh-STO as shown in Figures 3(b) and 3(c), the chemical shifts induced by Rh-doping for Ti 2p peaks are larger compared to that of the Sr 3d

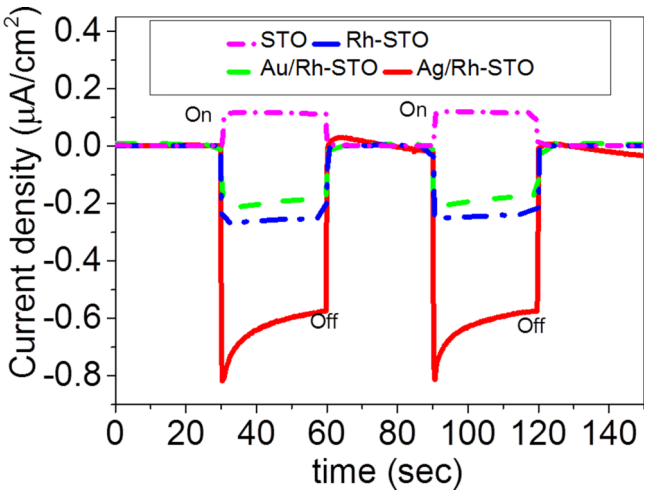

FIG. 2. Photocurrent densities with time for various STO films at zero bias voltage.

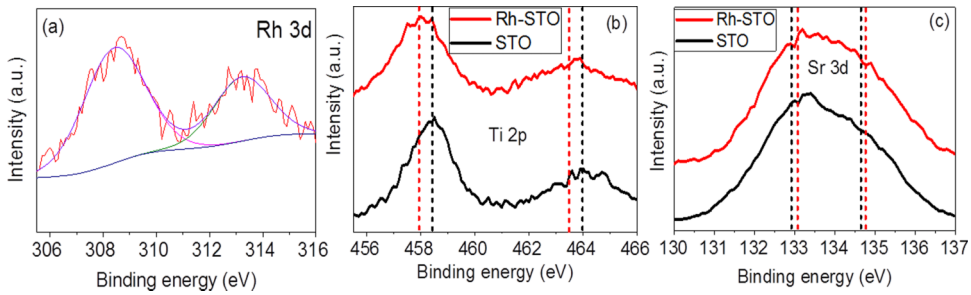

FIG. 3. XPS spectra of (a) Rh 3d, (b) Ti 2p, and (c) Sr 3d. Spectra of STO and Rh-STO. (Dotted lines represent the peak position values of the constituent peaks after the fitting). (The fit results are presented in Figure S2 and table S1 of the supplementary material).[32]

states. This indicates that substitution by Rh takes place preferentially at Ti^{4+} sites rather than at the Sr^{2+} sites which are in agreement with the XRD results.

The short circuit photocurrents of STO, Rh-STO, Au/Rh-STO, and Ag/Rh-STO were measured at various wavelengths (Figure S3 of the supplementary material),[32] to plot the action spectrum of

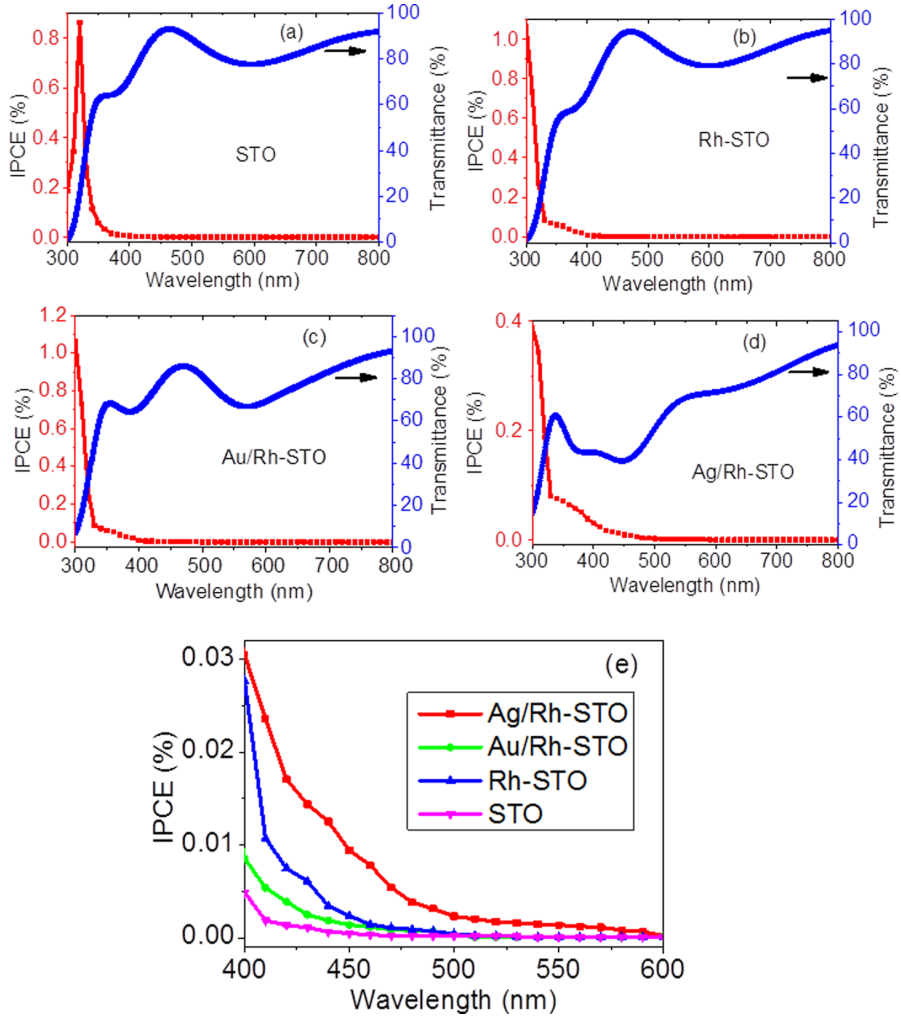

FIG. 4. IPCE spectrum and transmission spectra of (a) STO, (b) Rh-STO, (c) Au/Rh-STO, and (d) Ag/Rh-STO films. (e) Comparison of IPCE spectra. IPCE curve plotted using absolute values of the current density (Figure S3 of the supplementary material)[32] and light intensity (Figure S4 of the supplementary material).[32]

incident photon-to-current efficiency (IPCE) vs. photon wavelength as shown in Figures 4(a)-4(d). The transmittance spectrum was also plotted with action spectrum which is observed to be almost correlated in all the cases. Furthermore, a comparison of IPCE values is shown from 400 to 600 nm for all the photoelectrodes in Figure 4(e) where a visible light enhancement is seen with Rh doping and is further increased by the loading of Ag nanoparticles. The enhancement observed in the region from 400 to 470 nm in the case of Ag/Rh-STO could be related to plasmon from the small (<10 nm) Ag nanoparticles. Also a measurable photoresponse was observed in the visible range up to 600 nm, which is due to aggregated (>10 nm) particles. Whereas in the case of Au, a measurable photoresponse was observed only up to 530 nm.

STO is an n-type semiconductor where the majority charge carriers are electrons. Generally in n-type semiconductors, due to the built-in electric field, the electrons flow towards the bulk (ITO in our case) and this results in anodic photocurrent. Whereas in case of Rh-STO, which is aligned p-type with respect to the solution, the electrons flow towards the electrolyte solution.[25] As seen from the IPCE spectrum, loading Ag and Au nanoparticles facilitates the generation of hot carriers at wavelength longer than 400 nm and most possibly also promotes the charge separation under the influence of Schottky barrier at the metal STO interface.

As seen from Figures 4(d) and 4(e) and (Figure S3(d) of the supplementary material),[32] Ag/Rh-STO shows enhancement in the visible range. We believe that there are two possible pathways in which the charge transfer could occur leading to visible light enhancement in Ag/Rh-STO films. It has been noted earlier that Ag plasmons exert intense electric field in the local spot region.[26,27] In our case, a strong local electric field on the Rh-STO films is exhibited by the presence of Ag plasmon particularly in the range of 400-480 nm. Due to this intense electric field, the electrons are excited from the deep Rh^{3+} dopant level to conduction band near the Ag/STO interface region thereby facilitating the flow of cathodic photocurrent from the STO surface to the solution. It has been known that the hot electrons with energies higher than the Schottky barrier energy can be injected from the Fermi level (of the metal) to the conduction band of n-type semiconductor. By contrast, for the case of p-type semiconductor, the energy barrier (Φ_{B2}) between Fermi level and the top of valence band is smaller than the energy barrier (Φ_{B1}) between Fermi level and the bottom of conduction band; in our case, the values for Φ_{B1} and Φ_{B2} are calculated to be 2.2-2.4 eV and 0.8

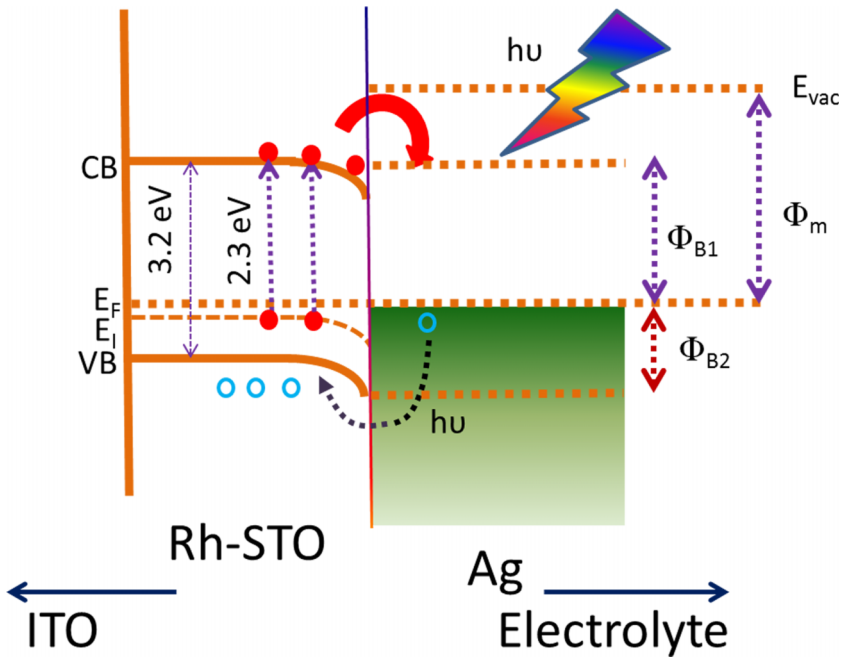

FIG. 5. Schematic illustration of the visible light photocurrent activity of Ag/Rh-STO (E_i—impurity level of Rh^{3+}, E_F—Fermi level, Φ_{B1}—barrier for electrons, Φ_{B2}—barrier for holes (Φ_{B1} = 2.2–2.4 eV and Φ_{B2} = 0.8–1.0 eV) and E_{vac} vacuum energy level with respect to Ag Fermi level (Φ_m = 4.5–4.7 eV)).

to 1.0 eV ($\Phi_{B1} > \Phi_{B2}$) assuming that the Fermi energy level for Rh-STO is close to Rh^{3+} doping level[28] and the work function of the silver is 4.5–4.7 eV.[29] Hence, here hot holes become major carriers to overcome the Schottky barrier and generate cathodic photocurrents[30,31] (see Fig. 5). Furthermore, we believe that the injection of hot holes into the valence band of Rh-STO must have been taken place to meet the charge compensation. Indeed, this process can be highly promoted in the presence of strong electromagnetic field (more than tenfold compared to incident light field amplitude) at the STO-Ag interface originating from LSPR of Ag NPs (supplementary material (Figure S5)).[32] There will be hot electron injection from Ag to STO but the excited electron falls back again into the Ag Fermi level leading to the cancellation of the charge separation and carrier movements. Regarding the Au/Rh-STO, the LSPR energy (ca. 600 nm) is lower than the Schottky barrier of Au/STO interface, and furthermore, factor such as migration of Au atoms into STO might also deteriorate the photoresponse.

In conclusion, we have fabricated smooth nanometer-thick $SrTiO_3$ films by wet chemical route and have studied the photocurrent characteristics of the pristine STO, Rh-doped STO, and Ag/Rh-STO. A cathodic photocurrent was observed with Rh-doped STO and it was further enhanced effectively with Ag nanoparticle loading. The IPCE spectrum correlates well with the absorption spectrum taken from each photoelectrode. Especially, the effect of Ag LSPR excitation energy on the visible catalytic activity was clearly demonstrated. The present work exemplifies the synergetic effect of localized surface plasmon resonance and impurity doping on the catalytic activity enhancement of the oxide catalyst. The results presented here will provide useful information towards the development of effective PEC cell operative under the solar light illumination.

[1] A. Fujishima and K. Honda, Nature **238**, 37 (1972).
[2] K. Hashimoto, H. Irie, and A. Fujishima, Jpn. J. Appl. Phys., Part 1 **44**, 8269 (2005).
[3] Y. Wang, R. Shi, J. Lin, and Y. Zhu, Energy Environ. Sci. **4**, 2922 (2011).
[4] T. K. Townsend, E. M. Sabio, N. D. Browning, and F. E. Osterloh, Energy Environ. Sci. **4**, 4270 (2011).
[5] A. B. Djurišić, Y. H. Leung, and A. M. C. Ng, Mater. Horiz. **1**, 400 (2014).
[6] H. Tong, S. X. Ouyang, Y. P. Bi, N. Umezawa, M. Oshikiri, and J. H. Ye, Adv. Mater. **24**, 229 (2012).
[7] H. Park, Y. Park, W. Kim, and W. Choi, J. Photochem. Photobiol., C **15**, 1 (2013).
[8] H. Yu, S. Ouyang, S. Yan, Z. Li, T. Yu, and Z. Zou, J. Mater. Chem. **21**, 11347 (2011).
[9] P. Reunchan, S. Ouyang, N. Umezawa, H. Xu, Y. Zhang, and J. Ye, J. Mater. Chem. A **1**, 4221 (2013).
[10] D. F. Wang, J. H. Ye, T. Kato, and T. Kimura, J. Phys. Chem. B **110**, 15824 (2006).
[11] Z. Jiao, T. Chen, J. Xiong, T. Wang, G. Lu, J. Ye, and Y. Bi, Sci. Rep. **3**, 02720 (2013).
[12] D. Hou, X. Hu, W. Ho, P. Hu, and Y. Huang, J. Mater. Chem. A **3**, 3935 (2015).
[13] R. Konta, T. Ishii, H. Kato, and A. Kudo, J. Phys. Chem. B **108**, 8992 (2004).
[14] K. Iwashina and A. Kudo, J. Am. Chem. Soc. **133**, 13272 (2011).
[15] J. Hirayama, R. Abe, and Y. Kamiya, Appl. Catal., B **144**, 721 (2014).
[16] H. Kato, Y. Sasaki, N. Shirakura, and A. Kudo, J. Mater. Chem. A **1**, 12327 (2013).
[17] S. Kawasaki, K. Nakatsuji, J. Yoshinobu, F. Komori, R. Takahashi, M. Lippmaa, K. Mase, and A. Kudo, Appl. Phys. Lett. **101**, 033910 (2012).
[18] C. Clavero, Nat. Photonics **8**, 95–103 (2014).
[19] X. M. Zhang, Y. L. Chen, R.-S. Liu, and D. P. Tsai, Rep. Prog. Phys. **76**, 046401 (2013).
[20] Y. Tian and T. Tatsuma, J. Am. Chem. Soc. **127**, 7632 (2005).
[21] R. Kodiyath, M. Manikandan, L. Liu, G. V. Ramesh, S. Koyasu, M. Miyauchi, Y. Sakuma, T. Tanabe, T. Gunji, T. D. Dao, S. Ueda, T. Nagao, J. Ye, and H. Abe, Chem. Commun. **50**, 15553 (2014).
[22] L. Liu, P. Li, B. Adisak, S. Ouyang, N. Umezawa, J. Ye, R. Kodiyath, T. Tanabe, G. V. Ramesh, and S. Ueda, J. Mater. Chem. A **2**, 9875 (2014).
[23] T. D. Dao, G. Han, N. Arai, T. Nabatame, Y. Wada, C. V. Hoang, M. Aono, and T. Nagao, Phys. Chem. Chem. Phys. **17**, 7395 (2015).
[24] H. Nishi, T. Torimoto, and T. Tatsuma, Phys. Chem. Chem. Phys. **17**, 4042 (2015).
[25] J. Cao, Y. Zhang, L. Liu, and J. Ye, Chem. Commun. **49**, 3440 (2013).
[26] H. Li, W. Lu, J. Tian, Y. Luo, A. M. Asiri, A. O. Al-Youbi, and X. Sun, Chem. - Eur. J. **18**, 8508 (2012).
[27] Z. Liu, W. Hou, P. Pavaskar, M. Aykol, and S. B. Cronin, Nano Lett. **11**, 1111 (2011).
[28] A. Kudo and Y. Miseki, Chem. Soc. Rev. **38**, 253 (2009).
[29] H. B. Michaelson, J. Appl. Phys. **48**, 4729 (1977).
[30] A. O. Govorov, H. Zhang, and Y. K. Gunko, J. Phys. Chem. C **117**, 16616 (2013).
[31] R. Sundararaman, P. Narang, A. S. Jermyn, W. A. Goddard III, and H. A. Atwater, Nat. Commun. **5**, 5788 (2014).
[32] See supplementary material at http://dx.doi.org/10.1063/1.4935305 for XRD patterns, binding energy values of XPS spectrum, photocurrent action spectrum, and field amplitude map.